

# Non-Hermitian dynamics of Cooper pair splitter

E. S. Ma and Z. Song\*

*School of Physics, Nankai University, Tianjin 300071, China*

We propose a non-Hermitian model for Cooper pair splitters, in which the process of electron tunneling into electrodes is characterized by non-Hermitian terms. We find that across a broad range of parameters, the energy levels consistently remain real, and coalescing states are always present. The Coulomb repulsion between electrons in a quantum dot affects the order of the coalescing states. This gives rise to two distinct dynamic behaviors: (i) when the initial state is an empty state, the final state supports a nonzero electron-escaping rate; (ii) the electron-escaping rate is zero for a single-electron initial state. In the former case, our exact solutions reveal that the average electron-escaping rate vanishes along a set of hyperbolic curves in the plane of the chemical potentials of the two quantum dots. The stability of the results in the presence of disordered perturbation is also investigated. Our findings pave the way for investigating Cooper pair splitters within the framework of non-Hermitian quantum mechanics.

## I. INTRODUCTION

Rigorous results for a model Hamiltonian play an important role in physics and sometimes open new avenues for exploration in the field. The exact solution to the quantum harmonic oscillator has played a crucial role in the history of physics. It stands as a key concept in traditional quantum mechanics and continues to be a cornerstone for modern research and applications within the field. One recent example is the discovery of the solution for the non-Hermitian harmonic oscillator, which serves as the foundation for  $\mathcal{PT}$ -symmetric quantum mechanics [1–4]. In traditional quantum mechanics, the Hamiltonian being Hermitian is a fundamental postulate that ensures that the energy spectrum is real and that the system undergoes unitary time evolution [5]. In contrast, the real spectrum and unitary dynamics are not required to be tied together in an open system. In recent years, non-Hermitian physics [6–10] has attracted much attention from various research areas [11–20]. Non-Hermitian quantum physics is particularly relevant for describing open quantum systems that interact with their environment, leading to phenomena such as damping probability and the appearance of nonorthogonal states.

Cooper pair splitters are devices that can separate Cooper pairs [21, 22], which are pairs of electrons that are bound together in a superconducting state, into individual electrons while maintaining their quantum entanglement. It has been explored in various experimental setups, including those based on nanowires [23–33], carbon nanotubes [34–37], graphene [38–41], and semiconductor quantum dots [33, 42]. These devices have shown promising results in generating entangled electrons, which are essential for quantum applications. Theoretical investigations are usually performed within the framework of Hermitian quantum mechanics [43–47]. However, it is a typical open system [48] in which the superconductor and electrodes can be considered as the electron source and

drains. From a theoretical point of view, a non-Hermitian Hamiltonian is a suitable candidate to characterize this system. Traditionally, Cooper pair splitters have been modeled using Hermitian quantum mechanics. However, it is crucial to propose a paradigm shift by incorporating non-Hermitian effects into our analysis. These effects are essential for capturing the nonreciprocal nature of the electron tunneling process.

In this work, we introduce a non-Hermitian model to analyze the behavior of a Cooper pair splitter, a device critical for the manipulation of electron pairs in open quantum systems. By incorporating non-Hermitian terms into the Hamiltonian, we aim to provide a more comprehensive understanding of the electron tunneling process and its implications for the energy levels and dynamics of the system. Through the exact solutions of the non-Hermitian Hamiltonian, we find that the energy levels in our non-Hermitian model consistently remain real, indicating the stability of the system. Moreover, we identify the presence of coalescing states, which are pivotal in understanding the dynamics of the electron-pair splitting process. Such dynamics are exclusive to non-Hermitian systems. We also find that the Coulomb repulsion between electrons in a quantum dot is a significant factor affecting the order of coalescing states. Our exact results demonstrate that the average electron-escaping rate decreases along a set of hyperbolic curves in the chemical potential plane of the two quantum dots. This finding offers a clear indication of the interplay among non-Hermitian effects, Coulomb repulsion, and dynamics.

This paper is organized as follows. In Section II, we introduce the Hamiltonian of the non-Hermitian Cooper pair splitter and provide the complete exact solutions. In Section III, we discuss two types of dynamics for two representative initial states. Two observables are defined to characterize the dynamics. The robustness of the dynamics under the time-dependent disorder perturbation is investigated in Section IV. Finally, we draw conclusions in Section V. Some details of the derivations are provided in the Appendix.

---

\* songtc@nankai.edu.cn

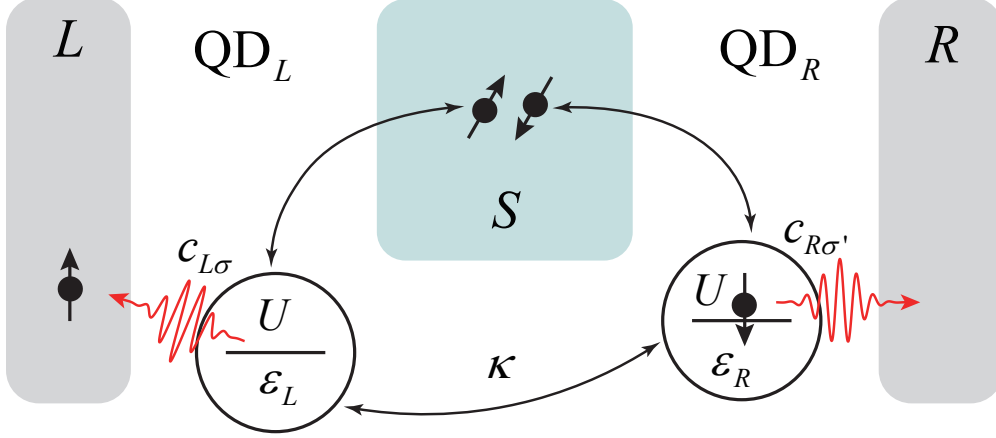


FIG. 1. The schematic depicts a Cooper pair splitter as described by the Hamiltonian in Eq. (1).  $S$  represents a superconductor, which serves as the source of Cooper pairs. Each quantum dot is represented by black circles, with respective chemical potentials  $\varepsilon_L$  and  $\varepsilon_R$ . The Hubbard on-site interaction is denoted by  $U$ . The hopping strength between two quantum dots is denoted by  $\kappa$ .  $L$  and  $R$  represent the left and right electrodes, respectively. The process of electrons escaping from quantum dots is characterized by the non-Hermitian term in Eq. (3).

## II. MODEL AND PHASE DIAGRAM

We begin with a non-Hermitian Cooper pair splitter, and the Hamiltonian is

$$H = H_1 + H_2, \quad (1)$$

with

$$H_1 = -\kappa \sum_{\sigma} c_{L\sigma}^{\dagger} c_{R\sigma} - \gamma d_S^{\dagger} + \text{h.c.} \\ + \sum_{\ell\sigma} \varepsilon_{\ell} c_{\ell\sigma}^{\dagger} c_{\ell\sigma} + U \sum_{\ell} n_{\ell\uparrow} n_{\ell\downarrow}, \quad (2)$$

and

$$H_2 = \lambda \sum_{\ell\sigma} c_{\ell\sigma}, \quad (3)$$

where  $\varepsilon_{\ell}$  represents the energy level of quantum dots, which can be tuned by external gates and  $\ell = L, R$ .  $\sigma = \uparrow, \downarrow$  is the index of the electron spin.  $d_S^{\dagger} = (c_{L\downarrow}^{\dagger} c_{R\uparrow}^{\dagger} - c_{L\uparrow}^{\dagger} c_{R\downarrow}^{\dagger}) / \sqrt{2}$  describes a singlet state. The amplitudes for Cooper pair splitting and elastic cotunneling are dominated by  $\gamma$  and  $\kappa$ , respectively.  $U$  is the interdot Coulomb potential and we consider  $U \gg \kappa, \gamma, \lambda$  for simplicity.  $H_2$  is the non-Hermitian term, which is responsible for transmitting split electrons from quantum dots to electrodes. A schematic of the system is displayed in Fig. 1.

The correlation between two electrons stems from the on-site Hubbard interaction  $U$ , which is crucial for understanding phenomena such as the Mott transition, antiferromagnetism, and superconductivity. To characterize the strong electron correlations, an effective Hamiltonian, such as the  $t - J$  Hamiltonian, can be derived by

using the Schrieffer-Wolff transformation [49], with the transformation generator depending on  $t/U$  and excluding the possibility for electrons to doubly occupy a single site [50].

The effective Hamiltonian reads

$$H_{\text{eff}} = \sum_{\ell\sigma} \varepsilon_{\ell} \tilde{c}_{\ell\sigma}^{\dagger} \tilde{c}_{\ell\sigma} - \kappa \sum_{\sigma} (\tilde{c}_{L\sigma}^{\dagger} \tilde{c}_{R\sigma} + \text{h.c.}) + \lambda \sum_{\ell\sigma} c_{\ell\sigma} \\ + J_{\text{eff}} \left( \mathbf{s}_L \cdot \mathbf{s}_R - \frac{1}{4} \right) - \gamma (d_S^{\dagger} + d_S), \quad (4)$$

where the exchange coupling strength  $J_{\text{eff}} = 4U\kappa^2 / [U^2 - (\varepsilon_L - \varepsilon_R)^2]$ , and  $s_{\ell}^{\alpha}$  ( $\alpha = x, y, z$ ) is the spin-1/2 operator. The operators  $\tilde{c}_{\ell\sigma}^{\dagger}$  and  $\tilde{c}_{\ell'\sigma'}$  satisfy the relations

$$\{\tilde{c}_{\ell\sigma}^{\dagger}, \tilde{c}_{\ell'\sigma'}\} = \delta_{\ell\ell'} \delta_{\sigma\sigma'}, \tilde{c}_{\ell\sigma}^{\dagger} \tilde{c}_{\ell\sigma}^{\dagger} = 0. \quad (5)$$

Based on the basis set

$$(1, d_S^{\dagger}, c_{L\uparrow}^{\dagger}, c_{R\uparrow}^{\dagger}, c_{L\downarrow}^{\dagger}, c_{R\downarrow}^{\dagger}) |0\rangle, \quad (6)$$

where  $|0\rangle$  is the vacuum state and satisfies  $c_{\ell\sigma} |0\rangle = 0$ , the matrix representation  $h$  of  $H_{\text{eff}}$  and the solution of equation

$$h\psi_n = \varepsilon_n \psi_n, h^{\dagger} \phi_n = \varepsilon_n^* \phi_n, \quad (7)$$

( $n \in [1, 6]$ ) are obtained in the appendix A. The analysis indicates that coalescing states [51] exist, and the number of these states depends on the system parameters. Specifically, finite values of  $U$  and infinite values of  $U$  lead to different degrees of energy level degeneracy and result in distinct EPs. The details are presented in the

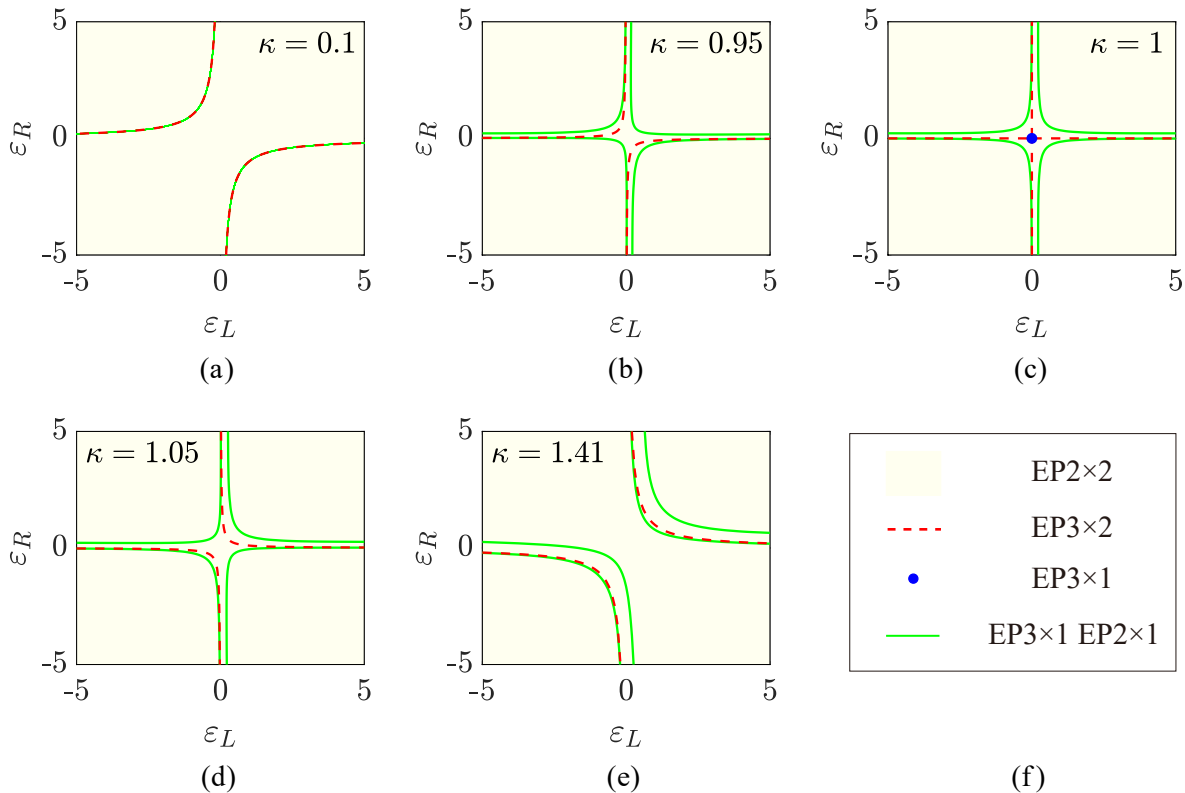


FIG. 2. The phase diagram for the Hamiltonian represented by Eq. (1) is depicted on the  $\varepsilon_L - \varepsilon_R$  parameter plane for several representative values of  $\kappa$  and  $U$  ( $\gamma = 1$ ). The configurations corresponding to the coalescing energy levels are indicated by color-coded regions or curves. For  $U = 20$ , the green solid lines indicate a 2nd-order EP and a 3rd-order EP. For  $U = \infty$ , the red dashed lines indicate two 3rd-order EPs.

appendix, and the structure of the solutions is demonstrated as a phase diagram in Fig. 2. Notably, except for the parameters at several hyperbolic curves in the phase diagram, the coalescing state lacks the components of the vacuum state  $|0\rangle$  and singlet pair state  $d_S^\dagger|0\rangle$ , while other eigenstates are superposition of all the basis states. This is crucial for the dynamics that will be discussed in the following section.

### III. TWO TYPES OF DYNAMICS

In this section, we will discuss the dynamics of such a non-Hermitian system. In general, there are two types of dynamics of a non-Hermitian system with a full real spectrum: (i) EP dynamics, in which the initial state is driven by a Jordan block. The corresponding final state approaches the coalescing state after long-term evolution. (ii) Quasi-Hermitian dynamics, the initial state is the superposition of a set of biorthonormal eigenstates and coalescing states. The evolved state is oscillatory, but the Dirac probability is nonconservative.

The solution of the present non-Hermitian Cooper-pair-splitter system indicates that two types of dynamics

are involved (see Appendix B) within the yellow region in the phase diagram. In the following, we introduce the electron-escaping rate, denoted by the following formula:

$$\mathcal{R}_{\ell\sigma}(t) = |\langle\psi(t)|c_{\ell\sigma}|\psi(t)\rangle|, \quad (8)$$

for an evolved state. Additionally, we define the average current as:

$$\mathcal{I}_{\ell\sigma} = \frac{1}{T} \int_0^T \mathcal{R}_{\ell\sigma}(t) dt, \quad (9)$$

to characterize the efficiency of the Cooper pair splitter. Here we consider the time evolution of two specific initial states for the yellow region in the phase diagram.

(i) The initial state is the vacuum state  $|\psi(0)\rangle = |0\rangle$ . Within the yellow region, where  $\xi_{1,2} \neq 0$ , we have

$$|\psi(0)\rangle = \sum_{i=1}^4 \alpha_i |\psi_i\rangle, \quad (10)$$

where the eigenstate  $|\psi_i\rangle$  denotes

$$\psi_i^T \left( 1, d_S^\dagger, c_{L\uparrow}^\dagger, c_{R\uparrow}^\dagger, c_{L\downarrow}^\dagger, c_{R\downarrow}^\dagger \right)^T |0\rangle. \quad (11)$$

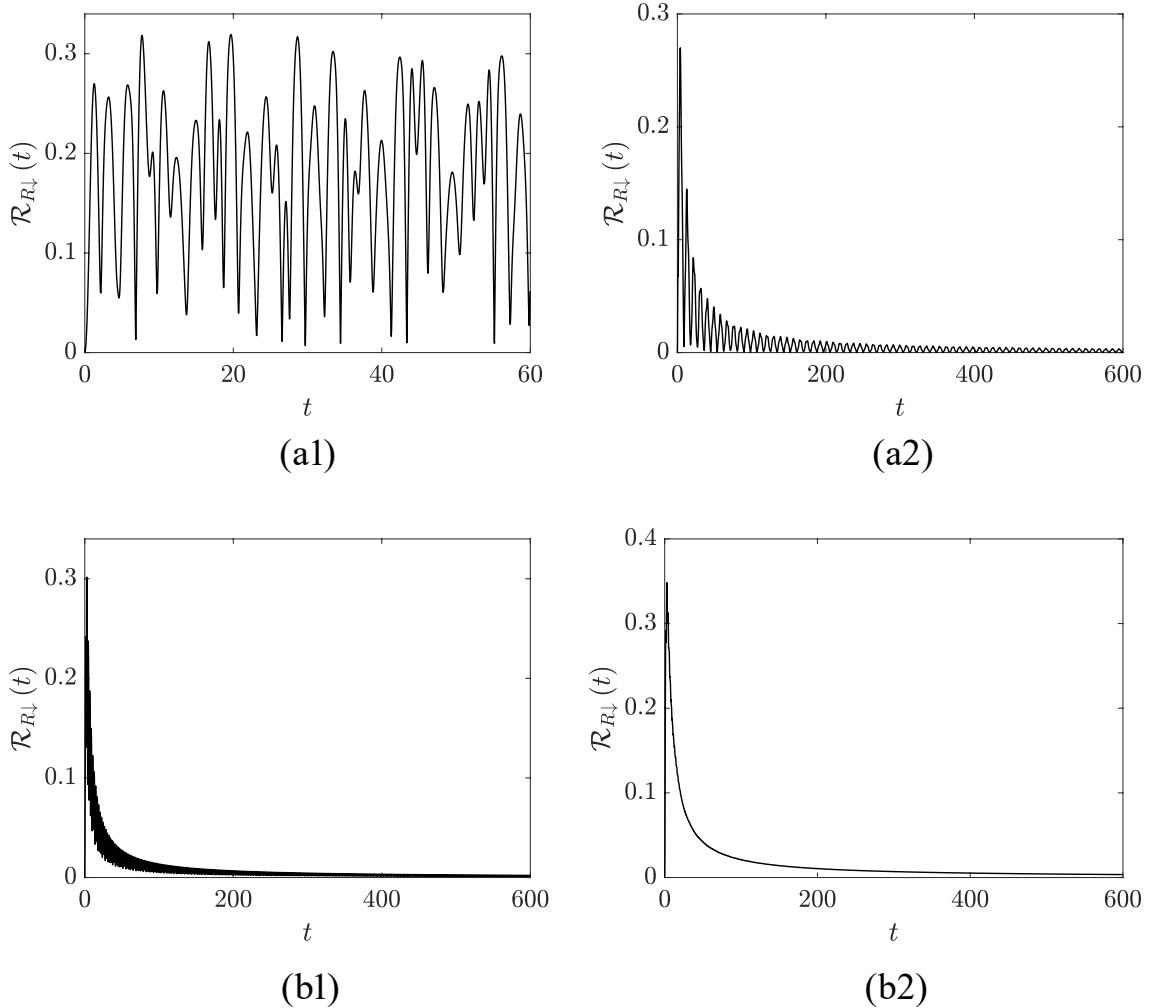


FIG. 3. The numerical results of the electron-escaping rate defined in Eq. (8). For  $U = 20$ , the initial state for (a1) and (a2) is  $|0\rangle$  and  $c_{L\uparrow}^\dagger |0\rangle$ , respectively. As expected, (a1) exhibits quasi-Hermitian dynamics and (b1) exhibits EP dynamics. Other parameters are  $\gamma = 1$ ,  $\lambda = 1$ ,  $\kappa = 1$ ,  $\varepsilon_L = 1$ , and  $\varepsilon_R = 2$ . The plots in (b1) and (b2) are the results for the same initial state  $|0\rangle$  but with  $U \rightarrow \infty$  for (b1) and  $U = 20$  for (b2). The parameters for (b1) are  $\gamma = 1$ ,  $\lambda = 1$ ,  $\kappa = 1.41$ ,  $\varepsilon_L = 0.5$ , and  $\varepsilon_R = 1.98$ , corresponding to the point located at the red dashed line in Fig. 2(e). The parameters for (b2) are  $\gamma = 1$ ,  $\lambda = 1$ ,  $\kappa = 1.41$ ,  $\varepsilon_L = 3.689$ , and  $\varepsilon_R = 0.239$ , corresponding to the point located at the green solid line in Fig. 2(e). The results agree with our predictions, corresponding to 2nd-order and 3rd-order EP dynamics, respectively.

The initial state is the superposition of two biorthonormal eigenstates  $\{|\psi_1\rangle, |\psi_2\rangle\}$  and two coalescing states  $\{|\psi_3\rangle, |\psi_4\rangle\}$ . Then the evolved state is

$$|\psi(t)\rangle = e^{-iHt} |\psi(0)\rangle = \sum_{i=1}^4 \alpha_i e^{-i\epsilon_i t} |\psi_i\rangle, \quad (12)$$

which is periodic, with its period determined by the energy levels  $\{\epsilon_i\}$ . Accordingly, we have

$$\mathcal{R}(t) \propto |\xi_1 f_1(t) + \xi_2 f_2(t)|, \quad (13)$$

where  $f_1(t)$  and  $f_2(t)$  are periodic functions.

(ii) The initial state is a single electron occupied state,  $|\psi(0)\rangle = c_{\ell\sigma}^\dagger |0\rangle$ . Within the yellow region, where  $\xi_{1,2} \neq$

0, we have

$$|\psi(t \rightarrow \infty)\rangle \propto (\mu |\psi_3\rangle + \nu |\psi_4\rangle) t. \quad (14)$$

Accordingly, we have

$$\mathcal{R}(t \rightarrow \infty) \rightarrow 0, \quad (15)$$

due to the fact

$$\langle \psi_i | c_{\ell\sigma} | \psi_j \rangle = 0, \quad (16)$$

if  $i, j = 3, 4$ . Now, we turn to the case beyond the yellow region, where the parameters satisfy Eq. (A18) for  $J_{\text{eff}} \neq 0$  and Eq. (A19) for  $J_{\text{eff}} = 0$ . In these situations, the

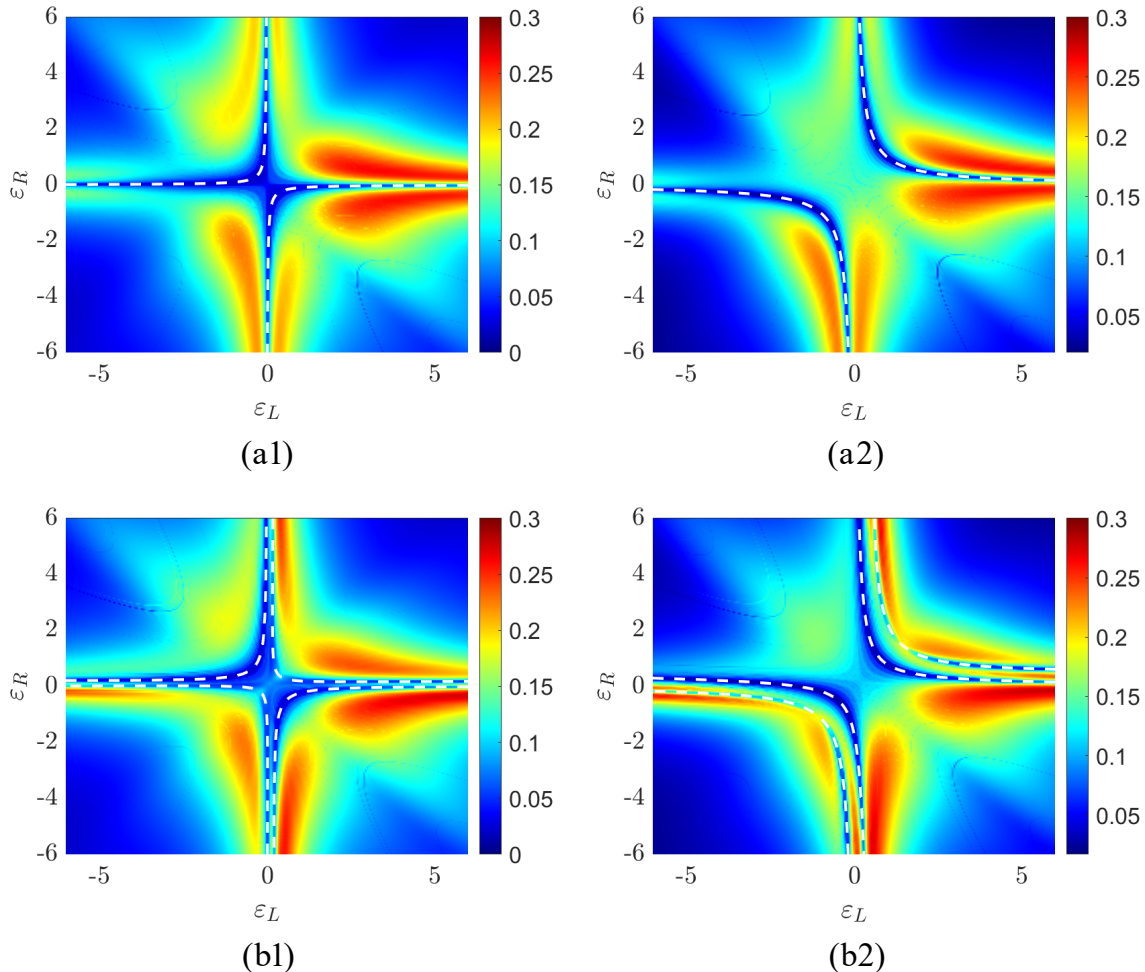


FIG. 4. Color contour plots of the numerical results for the average current  $\mathcal{I}_{R\downarrow}$  defined in Eq. (9). We take  $U \rightarrow \infty$  for (a1) and (a2) and  $U = 20$  for (b1) and (b2),  $\kappa = 0.95$  for (a1) and (b1) and  $\kappa = 1.41$  for (a2) and (b2). The initial state is  $|0\rangle$  and  $\gamma = 1$ ,  $\lambda = 1$  for all the cases. The white dashed lines represent the EP lines obtained from the exact results. We can see that the current is exactly zero along the EP lines for infinite  $U$ , and the current is relatively smaller along the EP lines for finite  $U$ . These results indicate that the current can demonstrate EP lines both for finite and infinite  $U$ .

time evolution of  $|\psi(0)\rangle = |0\rangle$  involves the Jordan block, which obeys EP dynamics. Accordingly, we have

$$\mathcal{R}(t \rightarrow \infty) \rightarrow 0, \quad (17)$$

which is distinct from the results observed in the yellow region.

Numerical simulations of the electron-escaping rate  $\mathcal{R}_{\ell\sigma}(t)$  for the system, using typical parameters, are performed to demonstrate our results. The evolved states, corresponding to two distinct types of initial states, can be obtained through numerically exact diagonalization. The results are presented in Fig. 3, which accords with our predictions.

Obviously, the average current is always zero for the initial state  $c_{\ell\sigma}^\dagger |0\rangle$  for any given system parameters. In contrast, it can be nonzero for the initial state  $|0\rangle$  and

nearly vanishes when a 2nd-order EP becomes a 3rd-order EP according to curves in Eq. (A18) for  $J_{\text{eff}} \neq 0$  and completely vanishes in Eq. (A19) for  $J_{\text{eff}} = 0$ . Fig. 4 shows the numerical results of the average current in the  $\varepsilon_L$ - $\varepsilon_R$  plane. We can see that the observable  $\mathcal{I}_{\ell\sigma}$  clearly demonstrates that the higher-order EPs appear in the non-Hermitian Cooper-pair-splitter system. Importantly, it also indicates that  $\mathcal{I}_{\ell\sigma}$  reaches its maximum in the vicinity of the zeros of  $\varepsilon_L$  or  $\varepsilon_R$ .

#### IV. STABILITY IN THE PRESENCE OF DISORDERED PERTURBATION

In this section, we focus on the situation involving a specific type of disorder and hope that the dynamics are

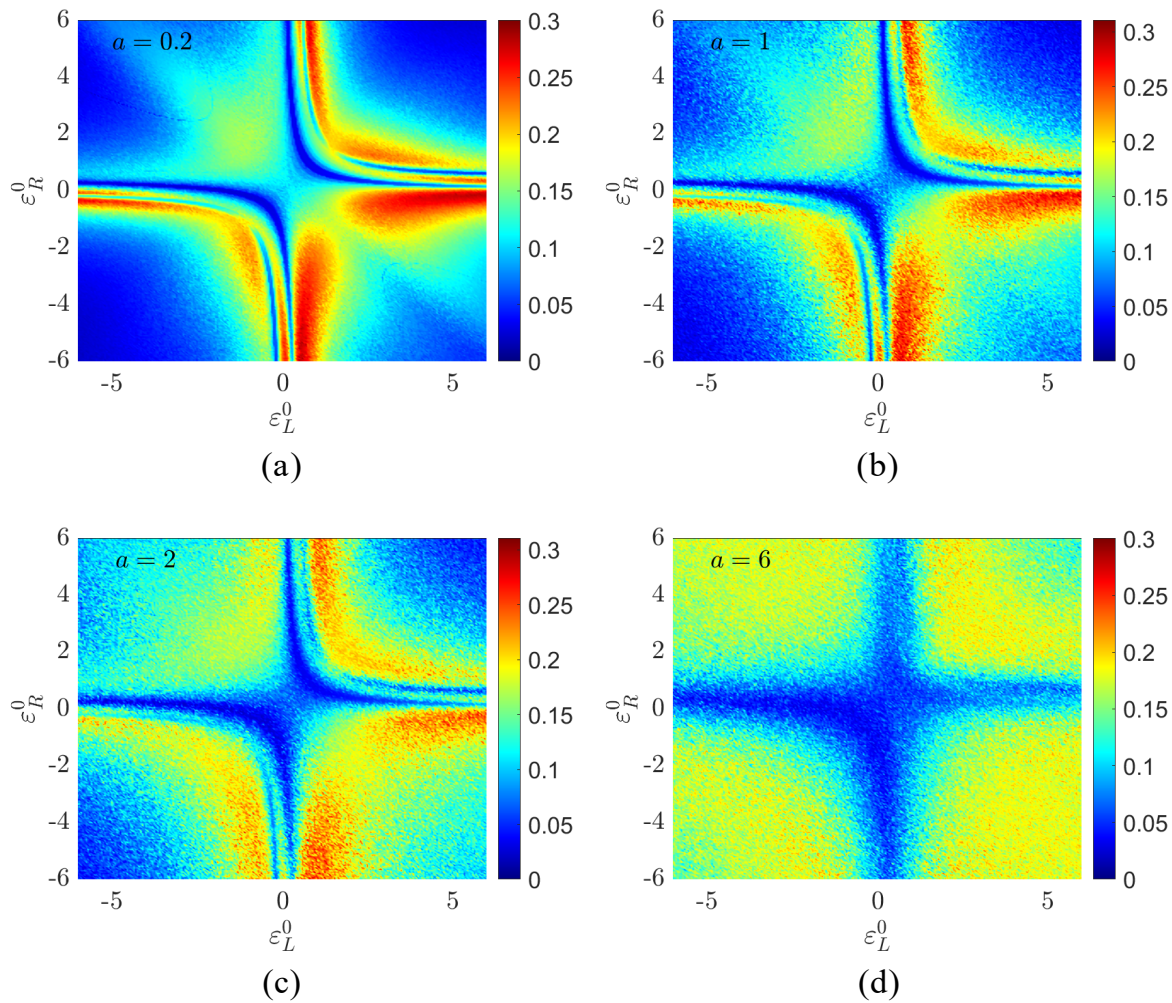


FIG. 5. Color contour plots of the average current for the time evolution of the initial state  $|0\rangle$  are driven by the Hamiltonian with time-dependent chemical potentials in Eq. (18). The numerical results are obtained from Eq. (21) with representative values of  $a$ . The other parameters are the same as those in Fig. 4(b2). This indicates that the exact results are robust against a certain range of disorder perturbations, and the difference between the cases with infinite and finite  $U$  disappears as  $a$  increases.

robust.

We consider the case where there are time-dependent random perturbations in the energy levels of quantum dots, which appear in the form

$$\varepsilon_{R,L}(t) = \varepsilon_{R,L}^0 + \text{ran}(-a, a)_t. \quad (18)$$

The notation  $\text{ran}(-a, a)_t$  represents a uniformly distributed random variable in the interval  $(-a, a)$ , resulting in the parameter  $\varepsilon_{R,L}(t)$  at time  $t$ . Due to the presence of the perturbation, it is difficult to obtain the exact evolved results. Numerical simulation is an efficient method for investigating this problem, and computations are performed on a uniform time mesh for discretization, i.e., stroboscopic time evolution. For a given initial state, the time-evolved state is computed by using

$$|\psi(t_n)\rangle = \mathcal{T} \prod_{i=1}^n e^{-iH(t_{i-1})(t_i - t_{i-1})} |\psi(0)\rangle, \quad (19)$$

where  $\mathcal{T}$  is the time-order operator and  $t_i - t_{i-1} = \delta t$  is a constant. Accordingly, the energy levels take the form

$$\varepsilon_{R,L}(t_i) = \varepsilon_{R,L}^0 + \text{ran}(-a, a)_i, \quad (20)$$

and the average current is computed by using

$$\mathcal{I}_{\ell\sigma} \approx \frac{1}{T} \sum_{i=1}^M |\langle \psi(t_i) | c_{\ell\sigma} | \psi(t_i) \rangle| \delta t. \quad (21)$$

The numerical results for the cases with finite Hubbard  $U$  and a range of representative values of  $a$  are plotted in Fig. 5. These results indicate that they remain robust against a certain range of perturbations. As  $a$  increases, the effect of finite  $U$  diminishes.

## V. SUMMARY

In summary, we introduced a non-Hermitian model to study the behavior of a Cooper pair splitter. The model incorporates non-Hermitian terms to describe the electron tunneling process into electrodes, capturing the nonreciprocal nature of this phenomenon. Our results reveal that within a wide parameter space, the energy levels of the system remain real and exhibit coalescing states. The presence of Coulomb repulsion between electrons in a quantum dot influences the ordering of these coalescing states, leading to two distinct dynamic behaviors. When the system starts in an empty state, the final state allows for a nonzero electron-escaping rate, indicating that electrons can be transferred to the electrodes. Conversely, if the system begins with a single-electron state, the electron-escaping rate is zero, suggesting a trapped state with no electron transfer. The exact solutions demonstrate that the average electron-escaping rate decreases along hyperbolic curves in the chemical potential plane of the two quantum dots, providing a unique signature of non-Hermitian dynamics. The findings not only contribute to the understanding of the Cooper pair splitter within the framework of non-Hermitian quantum mechanics but also open up new avenues for further research. Future work will explore the practical implications of these theoretical insights, including potential applications in quantum computing and quantum information processing.

## ACKNOWLEDGMENTS

This work was supported by the National Natural Science Foundation of China (under Grant No. 12374461).

## APPENDIX

In this appendix, we present a derivation for the solution to the Hamiltonian in Eq. (1), based on which the phase diagram in Fig. 2 can be obtained. In addition, we also provide a brief introduction to the dynamics driven by a Jordan block, which forms the foundational theory for our investigation in Sec. III.

### A. The solution to the Hamiltonian

In this subsection, we derive the effective Hamiltonian in Eq. (4) and provide its solutions. In the limit of a large Coulomb potential, where  $U \gg \lambda, \kappa, \gamma$ , the double-occupied states  $c_{L\uparrow}^\dagger c_{L\downarrow}^\dagger |0\rangle$  and  $c_{R\uparrow}^\dagger c_{R\downarrow}^\dagger |0\rangle$  can be neglected when considering low-energy eigenstates. To obtain the effective Hamiltonian for low-energy eigenstates, we consider the subspace constructed by the fol-

lowing basis

$$\left(1, d_S^\dagger, c_{L\uparrow}^\dagger, c_{R\uparrow}^\dagger, c_{L\downarrow}^\dagger, c_{R\downarrow}^\dagger\right) |0\rangle, \quad (\text{A1})$$

which forms a set of eigenstates of the sub-Hamiltonian  $H_0$ ,

$$H_0 = \sum_{\ell\sigma} \varepsilon_\ell c_{\ell\sigma}^\dagger c_{\ell\sigma} + U \sum_{\ell} n_{\ell\uparrow} n_{\ell\downarrow}. \quad (\text{A2})$$

Taking the hopping term

$$H' = -\kappa \sum_{\sigma} \left( c_{L\sigma}^\dagger c_{R\sigma} + \text{h.c.} \right), \quad (\text{A3})$$

as a perturbation, the effective Hamiltonian of  $H_0 + H'$  can be obtained as

$$H_0 + H' \rightarrow \sum_{\ell\sigma} \varepsilon_\ell \tilde{c}_{\ell\sigma}^\dagger \tilde{c}_{\ell\sigma} - \kappa \sum_{\sigma} \left( \tilde{c}_{L\sigma}^\dagger \tilde{c}_{R\sigma} + \text{h.c.} \right) + J_{\text{eff}} \left( \mathbf{s}_L \cdot \mathbf{s}_R - \frac{1}{4} \right), \quad (\text{A4})$$

where the exchange coupling strength

$$J_{\text{eff}} = \frac{4U\kappa^2}{U^2 - (\varepsilon_L - \varepsilon_R)^2}, \quad (\text{A5})$$

and the spin-1/2 operator is defined by

$$s_{\ell}^{\alpha} = \frac{1}{2} \left( \tilde{c}_{\ell\uparrow}^\dagger, \tilde{c}_{\ell\downarrow}^\dagger \right) \sigma^{\alpha} \begin{pmatrix} \tilde{c}_{\ell\uparrow} \\ \tilde{c}_{\ell\downarrow} \end{pmatrix}, \quad (\text{A6})$$

with  $\sigma^{\alpha}$  ( $\alpha = x, y, z$ ) being the Pauli matrix. The operators  $\tilde{c}_{\ell\sigma}^\dagger$  and  $\tilde{c}_{\ell'\sigma'}$  satisfy the relations

$$\left\{ \tilde{c}_{\ell\sigma}^\dagger, \tilde{c}_{\ell'\sigma'} \right\} = \delta_{\ell\ell'} \delta_{\sigma\sigma'}, \tilde{c}_{\ell\sigma}^\dagger \tilde{c}_{\ell\sigma}^\dagger = 0. \quad (\text{A7})$$

Together with the non-Hermitian and pairing terms we obtain the effective Hamiltonian

$$H_{\text{eff}} = \sum_{\ell\sigma} \varepsilon_\ell \tilde{c}_{\ell\sigma}^\dagger \tilde{c}_{\ell\sigma} - \kappa \sum_{\sigma} \left( \tilde{c}_{L\sigma}^\dagger \tilde{c}_{R\sigma} + \text{h.c.} \right) + \lambda \sum_{\ell\sigma} c_{\ell\sigma} + J_{\text{eff}} \left( \mathbf{s}_L \cdot \mathbf{s}_R - \frac{1}{4} \right) - \gamma \left( d_S^\dagger + d_S \right). \quad (\text{A8})$$

Now, we turn to the solution of the effective Hamiltonian,  $H_{\text{eff}}$ . Based on the basis set in Eq. (A1), the matrix representation of  $H_{\text{eff}}$  is obtained as

$$h = \begin{pmatrix} 0 & -\gamma & \lambda & \lambda & \lambda & \lambda \\ -\gamma & \varepsilon_R + \varepsilon_L - J_{\text{eff}} & 0 & 0 & 0 & 0 \\ 0 & \lambda/\sqrt{2} & \varepsilon_L & -\kappa & 0 & 0 \\ 0 & \lambda/\sqrt{2} & -\kappa & \varepsilon_R & 0 & 0 \\ 0 & -\lambda/\sqrt{2} & 0 & 0 & \varepsilon_L & -\kappa \\ 0 & -\lambda/\sqrt{2} & 0 & 0 & -\kappa & \varepsilon_R \end{pmatrix}. \quad (\text{A9})$$

The solution to the system satisfies the Schrodinger equations

$$h\psi_n = \varepsilon_n \psi_n, h^\dagger \phi_n = \varepsilon_n^* \phi_n, \quad (\text{A10})$$

( $n \in [1, 6]$ ). It is easy to check that the explicit forms of the eigenvectors and eigenvalues are

$$\psi_{1,2} = \begin{pmatrix} -\sqrt{2}\gamma\xi_{1,2}/\epsilon_{1,2} \\ \sqrt{2}\xi_{1,2} \\ \lambda(\kappa + \epsilon_R - \epsilon_{1,2}) \\ \lambda(\kappa + \epsilon_L - \epsilon_{1,2}) \\ -\lambda(\kappa + \epsilon_R - \epsilon_{1,2}) \\ -\lambda(\kappa + \epsilon_L - \epsilon_{1,2}) \end{pmatrix}, \quad (\text{A11})$$

and

$$\psi_3 = \psi_5, \psi_4 = \psi_6, \\ \psi_{3,4} = \begin{pmatrix} 0 \\ 0 \\ \kappa + \epsilon_R - \epsilon_{3,4} \\ \kappa + \epsilon_L - \epsilon_{3,4} \\ -(\kappa + \epsilon_R - \epsilon_{3,4}) \\ -(\kappa + \epsilon_L - \epsilon_{3,4}) \end{pmatrix}, \quad (\text{A12})$$

with

$$\epsilon_{1,2} = \frac{\epsilon_L + \epsilon_R - J_{\text{eff}} \pm \sqrt{(\epsilon_L + \epsilon_R - J_{\text{eff}})^2 + 4\gamma^2}}{2}, \\ \epsilon_3 = \epsilon_5, \epsilon_4 = \epsilon_6, \\ \epsilon_{3,4} = \frac{\epsilon_L + \epsilon_R \pm \sqrt{(\epsilon_L - \epsilon_R)^2 + 4\kappa^2}}{2}, \quad (\text{A13})$$

where the parameter is

$$\xi_{1,2} = \epsilon_{1,2}J_{\text{eff}} - \gamma^2 - \epsilon_L\epsilon_R + \kappa^2. \quad (\text{A14})$$

In parallel, we have

$$\phi_{1,2} = \begin{pmatrix} \xi_{1,2} \\ -\xi_{1,2}\epsilon_{1,2}/\gamma \\ \lambda(\epsilon_R - \epsilon_{1,2} + \kappa) \\ \lambda(\epsilon_L - \epsilon_{1,2} + \kappa) \\ \lambda(\epsilon_R - \epsilon_{1,2} + \kappa) \\ \lambda(\epsilon_L - \epsilon_{1,2} + \kappa) \end{pmatrix}, \quad (\text{A15})$$

and

$$\phi_3 = \phi_5, \phi_4 = \phi_6, \\ \phi_{3,4} = \begin{pmatrix} 0 \\ 0 \\ \epsilon_R - \epsilon_{3,4} + \kappa \\ \epsilon_L - \epsilon_{3,4} + \kappa \\ \epsilon_R - \epsilon_{3,4} + \kappa \\ \epsilon_L - \epsilon_{3,4} + \kappa \end{pmatrix}. \quad (\text{A16})$$

We note that all the energy levels  $\{\epsilon_n\}$  are real, and  $\psi_3$  and  $\psi_4$  are two 2nd-order coalescing states. This can also be confirmed by the identities

$$\phi_3^\dagger \psi_3 = \phi_4^\dagger \psi_4 = 0. \quad (\text{A17})$$

That is, the biorthogonal modes of two states are zero.

We conclude that, in general, the solution to the system consists of two real levels and two 2nd-order coalescing levels, except for the following case. The equation of  $\xi_1 = 0$  or  $\xi_2 = 0$  corresponds to the curve in the parameter  $\epsilon_L$ - $\epsilon_R$  plane, which is described by the following equation

$$J_{\text{eff}}^2 (\epsilon_L\epsilon_R - \kappa^2) + J_{\text{eff}} (\epsilon_L + \epsilon_R) \zeta + \zeta^2 = 0. \quad (\text{A18})$$

Here, the coefficient is defined as  $\zeta = \kappa^2 - \gamma^2 - \epsilon_L\epsilon_R$ . Under this condition, we find that one element of  $\{\epsilon_1, \epsilon_2\}$  is equal to one element of  $\{\epsilon_3, \epsilon_4\}$ , indicating the coalescence between one state of  $\{\psi_1, \psi_2\}$  and one state of  $\{\psi_3, \psi_4\}$ . Therefore, the solution of the system consists of one 2nd-order coalescing level and one 3rd-order coalescing level for  $\xi_{1,2} = 0$  when  $J_{\text{eff}}$  is not equal to zero.

When we consider the limit as  $U$  approaches infinity, and  $J_{\text{eff}}$  approaches 0, the energy levels remain real. The solution of the system consists of two real levels and two 2nd-order coalescing levels. Particularly, at the curve

$$\epsilon_L\epsilon_R = \kappa^2 - \gamma^2, \quad (\text{A19})$$

in the parameter  $\epsilon_L$ - $\epsilon_R$  plane, we have  $\zeta = 0$ , and then

$$\psi_1 = \psi_3 = \psi_5, \psi_2 = \psi_4 = \psi_6, \quad (\text{A20})$$

and

$$\phi_1 = \phi_3 = \phi_5, \phi_2 = \phi_4 = \phi_6. \quad (\text{A21})$$

The solution of the system consists of two 3rd-order coalescing levels, which can be confirmed by the identities

$$\phi_1^\dagger \psi_1 = \phi_2^\dagger \psi_2 = 0. \quad (\text{A22})$$

Accordingly, in the region where  $\kappa^2 - \gamma^2 > 0$ , the hyperbolic curves are in the first and third quadrants. Conversely, when  $\kappa^2 - \gamma^2 < 0$ , they are in the second and fourth quadrants. Specifically, under these conditions, two of the hyperbolic curves degenerate to lines along two principal axes

$$\epsilon_R = 0, \text{ or } \epsilon_L = 0, \quad (\text{A23})$$

at  $\kappa = \pm\gamma$ .

## B. EP dynamics

In this subsection, we present a general formalism for the temporal evolution of an initial state that includes a Jordan block. In non-Hermitian systems, an EP is a parameter value at which two or more eigenvalues and their corresponding eigenvectors coalesce. This is a point of non-Hermitian degeneracy where the usual spectral decomposition of the operator fails because the eigenvectors are no longer linearly independent.



Mathematically, an EP is always associated with a Jordan block corresponding to a single eigenvalue  $\lambda$ . This block has the form:

$$J_d = \begin{bmatrix} \lambda & 1 & 0 & \cdots & 0 \\ 0 & \lambda & 1 & \cdots & 0 \\ \vdots & \vdots & \ddots & \vdots & \vdots \\ 0 & 0 & \cdots & \lambda & 1 \\ 0 & 0 & \cdots & 0 & \lambda \end{bmatrix}, \quad (\text{B1})$$

which is a  $d \times d$  matrix, satisfying  $(J_d - \lambda)^d = 0$ .

Applying the above analysis to the solution for  $h$ , we have the following results. For the case with two 2nd-order EPs, there exist two auxiliary states  $\psi_{3,4}^{\text{au}}$  that satisfy

$$(h - \epsilon_{3,4}) \psi_{3,4}^{\text{au}} = \psi_{3,4}. \quad (\text{B2})$$

Then, for an initial state with nonzero components of

$\psi_{3,4}^{\text{au}}$ , we have the long-term evolution

$$|\psi(t \rightarrow \infty)\rangle \propto (\mu |\psi_3\rangle + \nu |\psi_4\rangle) t. \quad (\text{B3})$$

On the other hand, for the case with two 3rd-order EPs, there exists four auxiliary states  $\{\psi_j^{\text{au}}, j \in [1, 4]\}$  obeying

$$(h - \epsilon_3) \psi_1^{\text{au}} = \psi_3^{\text{au}}, (h - \epsilon_3) \psi_3^{\text{au}} = \psi_3, \quad (\text{B4})$$

and

$$(h - \epsilon_4) \psi_2^{\text{au}} = \psi_4^{\text{au}}, (h - \epsilon_4) \psi_4^{\text{au}} = \psi_4. \quad (\text{B5})$$

Then, for an initial state with nonzero components of  $\psi_{1,2,3,4}^{\text{au}}$ , we have the long-term evolution

$$|\psi(t \rightarrow \infty)\rangle \propto (\beta_1 |\psi_3\rangle + \beta_2 |\psi_4\rangle) t^2. \quad (\text{B6})$$

- 
- [1] C. M. Bender and S. Boettcher, Real spectra in non-Hermitian Hamiltonians having  $\mathcal{PT}$  symmetry, *Phys. Rev. Lett.* **80**, 5243 (1998).
- [2] C. M. Bender, D. C. Brody, and H. F. Jones, Complex extension of quantum mechanics, *Phys. Rev. Lett.* **89**, 270401 (2002).
- [3] C. M. Bender, J. Brod, A. Refig, and M. E. Reuter, The C operator in  $\mathcal{PT}$ -symmetric quantum theories, *J. Phys. A: Math. Gen.* **37**, 10139 (2004).
- [4] C. M. Bender, Making sense of non-Hermitian Hamiltonians, *Rep. Prog. Phys.* **70**, 947–1018 (2007).
- [5] D. A. McQuarrie, *Quantum Chemistry*. University Science Books, Mill Valley, CA, 1983.
- [6] A. Mostafazadeh, Pseudo-Hermiticity versus  $\mathcal{PT}$ -symmetry: Equivalence of pseudo-Hermiticity and the presence of antilinear symmetries, *J. Math. Phys.* **43**, 205 (2002).
- [7] A. Mostafazadeh, Pseudo-Hermiticity versus  $\mathcal{PT}$ -symmetry II: Equivalence of pseudo-Hermiticity and the presence of antilinear symmetries, *J. Math. Phys.* **43**, 2814 (2002).
- [8] A. Mostafazadeh, Pseudo-Hermiticity versus  $\mathcal{PT}$ -symmetry III: Equivalence of pseudo-Hermiticity and the presence of antilinear symmetries, *J. Math. Phys.* **43**, 3944 (2002).
- [9] A. Mostafazadeh, Pseudo-supersymmetric quantum mechanics and isospectral pseudo-Hermitian Hamiltonians, *Nucl. Phys. B* **640**, 419 (2002).
- [10] A. Mostafazadeh, Pseudo-Hermiticity and generalized  $\mathcal{PT}$ - and  $\mathcal{CPT}$ -symmetries, *J. Math. Phys.* **44**, 974 (2003).
- [11] S. Longhi, Bloch oscillations in complex crystals with  $\mathcal{PT}$  symmetry, *Phys. Rev. Lett.* **103**, 123601 (2009).
- [12] L. Jin and Z. Song, Physics counterpart of the  $\mathcal{PT}$  non-Hermitian tight-binding chain, *Phys. Rev. A* **81**, 032109 (2010).
- [13] T. E. Lee and C.-K. Chan, Heralded magnetism in non-Hermitian atomic systems, *Phys. Rev. X* **4**, 041001 (2014).
- [14] L. Jin, Topological phases and edge states in a non-Hermitian trimerized optical lattice, *Phys. Rev. A* **96**, 032103 (2017).
- [15] C. Qin, B. Wang, Z. J. Wong, S. Longhi, and P. Lu, Discrete diffraction and Bloch oscillations in non-Hermitian frequency lattices induced by complex photonic gauge fields, *Phys. Rev. B* **101**, 064303 (2020).
- [16] Y. Ashida, Z. Gong, and M. Ueda, Non-Hermitian physics, *Adv. Phys.* **69**, 249 (2020).
- [17] L. Jin and Z. Song, Symmetry-protected scattering in non-Hermitian linear systems, *Chin. Phys. Lett.* **38**, 024202 (2021).
- [18] W. Zhang, X. Ouyang, X. Huang, X. Wang, H. Zhang, Y. Yu, X. Chang, Y. Liu, D.-L. Deng, and L.-M. Duan, Observation of non-Hermitian topology with nonunitary dynamics of solidstate spins, *Phys. Rev. Lett.* **127**, 090501 (2021).
- [19] J. Rohn, K. P. Schmidt, and C. Genes, Classical phase synchronization in dissipative non-Hermitian coupled systems, *Phys. Rev. A* **108**, 023721 (2023).
- [20] C. Liang, Y. Tang, A.-N. Xu, and Y.-C. Liu, Observation of exceptional points in thermal atomic ensembles, *Phys. Rev. Lett.* **130**, 263601 (2023).
- [21] G. B. Lesovik, T. Martin, and G. Blatter, Electronic entanglement in the vicinity of a superconductor, *Eur. Phys. J. B* **24**, 287 (2001).
- [22] P. Recher, E. V. Sukhorukov, and D. Loss, Andreev tunneling, Coulomb blockade, and resonant transport of non-local spin-entangled electrons, *Phys. Rev. B* **63**, 165314 (2001).
- [23] L. Hofstetter, S. Csonka, J. Nygård, and C. Schönberger, Cooper pair splitter realized in a two-quantum-dot Y-junction, *Nature* **461**, 960 (2009).
- [24] L. Hofstetter, S. Csonka, A. Baumgartner, G. Fülöp, S. d'Hollosy, J. Nygård, and C. Schönberger, Finite-Bias Cooper Pair Splitting, *Phys. Rev. Lett.* **107**, 136801 (2011).

- [25] A. Das, R. Ronen, M. Heiblum, D. Mahalu, A. V. Kretinin, and H. Shtrikman, High-efficiency Cooper pair splitting demonstrated by two-particle conductance resonance and positive noise cross-correlation, *Nat. Commun.* **3**, 1165 (2012).
- [26] G. Fülöp, S. d'Hollosy, A. Baumgartner, P. Makk, V. A. Guzenko, M. H. Madsen, J. Nygård, C. Schönenberger, and S. Csonka, Local electrical tuning of the nonlocal signals in a Cooper pair splitter, *Phys. Rev. B* **90**, 235412 (2014).
- [27] G. Fülöp, F. Domínguez, S. d'Hollosy, A. Baumgartner, P. Makk, M. H. Madsen, V. A. Guzenko, J. Nygård, C. Schönenberger, A. Levy Yeyati, and S. Csonka, Magnetic Field Tuning and Quantum Interference in a Cooper Pair Splitter, *Phys. Rev. Lett.* **115**, 227003 (2015).
- [28] S. Baba, C. Jünger, S. Matsuo, A. Baumgartner, Y. Sato, H. Kamata, K. Li, S. Jeppesen, L. Samuelson, H. Q. Xu, C. Schönenberger, and S. Tarucha, Cooper-pair splitting in two parallel InAs nanowires, *New J. Phys.* **20**, 063021 (2018).
- [29] Z. Scherübl, G. Fülöp, J. Gramich, A. Pályi, C. Schönenberger, J. Nygård, and S. Csonka, From Cooper pair splitting to nonlocal spectroscopy of a Shiba state, *Phys. Rev. Res.* **4**, 023143 (2022).
- [30] O. Kürtössy, Z. Scherübl, G. Fülöp, I. E. Lukács, T. Kanne, J. Nygård, P. Makk, and S. Csonka, Parallel InAs nanowires for Cooper pair splitters with Coulomb repulsion, *npj Quantum Mater.* **7**, 88 (2022).
- [31] A. Bordoloi, V. Zannier, L. Sorba, C. Schönenberger, and A. Baumgartner, Spin cross-correlation experiments in an electron entangler, *Nature* **612**, 454 (2022).
- [32] G. Wang, T. Dvir, G. P. Mazur, C.-X. Liu, N. van Loo, S. L. D. ten Haaf, A. Bordin, S. Gazibegovic, G. Badawy, E. P. A. M. Bakkers, M. Wimmer, and L. P. Kouwenhoven, Singlet and triplet Cooper pair splitting in hybrid superconducting nanowires, *Nature* **612**, 448 (2022).
- [33] D. de Jong, C. G. Prosko, L. Han, F. K. Malinowski, Y. Liu, L. P. Kouwenhoven, and W. Pfaff, Controllable Single Cooper Pair Splitting in Hybrid Quantum Dot Systems, *Phys. Rev. Lett.* **131**, 157001 (2023).
- [34] L. G. Herrmann, F. Portier, P. Roche, A. L. Yeyati, T. Kontos, and C. Strunk, Carbon Nanotubes as Cooper-Pair Beam Splitters, *Phys. Rev. Lett.* **104**, 026801 (2010).
- [35] J. Schindele, A. Baumgartner, and C. Schönenberger, Near-Unity Cooper Pair Splitting Efficiency, *Phys. Rev. Lett.* **109**, 157002 (2012).
- [36] L. G. Herrmann, P. Buset, W. J. Herrera, F. Portier, P. Roche, C. Strunk, A. Levy Yeyati, and T. Kontos, Spectroscopy of non-local superconducting correlations in a double quantum dot, arXiv:1205.1972.
- [37] L. E. Bruhat, T. Cubaynes, J. J. Viennot, M. C. Dartailh, M. M. Desjardins, A. Cottet, and T. Kontos, Circuit QED with a quantum-dot charge qubit dressed by Cooper pairs, *Phys. Rev. B* **98**, 155313 (2018).
- [38] Z. B. Tan, D. Cox, T. Nieminen, P. Lähteenmäki, D. Golubev, G. B. Lesovik, and P. J. Hakonen, Cooper Pair Splitting by Means of Graphene Quantum Dots, *Phys. Rev. Lett.* **114**, 096602 (2015).
- [39] I. V. Borzenets, Y. Shimazaki, G. F. Jones, M. F. Craciun, S. Russo, M. Yamamoto, and S. Tarucha, High Efficiency CVD Graphene-lead (Pb) Cooper Pair Splitter, *Sci. Rep.* **6**, 23051 (2016).
- [40] Z. B. Tan, A. Laitinen, N. S. Kirsanov, A. Galda, V. M. Vinokur, M. Haque, A. Savin, D. S. Golubev, G. B. Lesovik, and P. J. Hakonen, Thermoelectric current in a graphene Cooper pair splitter, *Nat. Commun.* **12**, 138 (2021).
- [41] P. Pandey, R. Danneau, and D. Beckmann, Ballistic Graphene Cooper Pair Splitter, *Phys. Rev. Lett.* **126**, 147701 (2021).
- [42] A. Bordin, X. Li, D. van Driel, J. C. Wolff, Q. Wang, S. L. D. ten Haaf, G. Wang, N. van Loo, L. P. Kouwenhoven, and T. Dvir, Crossed Andreev reflection and elastic cotunneling in a three-site Kitaev chain nanowire device, arXiv:2306.07696.
- [43] B. Hiltcher, M. Governale, J. Splettstoesser, and J. König, Adiabatic pumping in a double-dot Cooperpair beam splitter, *Phys. Rev. B* **84**, 155403 (2011).
- [44] F. Brange, K. Prech, and C. Flindt, Dynamic Cooper Pair Splitter, *Phys. Rev. Lett.* **127**, 237701 (2021).
- [45] J. Eldridge, M. G. Pala, M. Governale, and J. König, Superconducting proximity effect in interacting double-dot systems, *Phys. Rev. B* **82**, 184507 (2010).
- [46] N. Walldorf, F. Brange, C. Padurariu, and C. Flindt, Noise and full counting statistics of a Cooper pair splitter, *Phys. Rev. B* **101**, 205422 (2020).
- [47] F. Brange, R. Baruah, and C. Flindt, Adiabatic Cooper pair splitter, *Phys. Rev. B* **109**, L081402 (2024).
- [48] O. Sauret, D. Feinberg, and T. Martin, Quantum master equations for the superconductor-quantum dot entangler, *Phys. Rev. B* **70**, 245313 (2004).
- [49] S. Bravyi, D. P. DiVincenzo, and D. Loss, Schrieffer-Wolff transformation for quantum many-body systems, *Ann. Phys.* **326**, 2793 (2011).
- [50] H.-P. Eckle, *Models of Quantum Matter* (Oxford University Press, Oxford, 2019).
- [51] N. Moiseyev, *Non-Hermitian Quantum Mechanics* (Cambridge University Press, Cambridge, U.K., 2011).